UPPSALA
UNIVERSITET

UPTEC F13037
Examensarbete 30 hp
Oktober 2013

Modeling a novel sorption dehumidification method

super saturation of water vapour in a closed volume using the finite volume method

Per Dahlbäck

UPPSALA
UNIVERSITET

Teknisk- naturvetenskaplig fakultet
UTH-enheten

Besöksadress:
Ångströmlaboratoriet
Lägerhyddsvägen 1
Hus 4, Plan 0

Postadress:
Box 536
751 21 Uppsala

Telefon:
018 – 471 30 03

Telefax:
018 – 471 30 00

Hemsida:
http://www.teknat.uu.se/student

Abstract

Modeling a novel sorption dehumidification method, super saturation of water vapour in a closed volume using the finite volume method

Per Dahlbäck

This thesis develops and evaluates a method to simulate energy consumption and water production for a novel sorption dehumidification process. The system consists of a chamber comprising a hygroscopic material and a heating device. The process consists of an adsorption phase and a regeneration phase. For both the regeneration phase and the adsorption phase the model considers the heat distribution by thermal diffusion and convection and the water transport by diffusion and convection. For the regeneration phase the radiation is also considered since the radiative power increases with temperature to the power of four. Further, a model for the condensation process is implemented and a model for the condensation is suggested. To model the properties of the hygroscopic materials, the adsorption curves for SiO2 and AlO2 are investigated.
The model were evaluated by comparing the simulated values with experimental measurements.

The results from the the simulation of the regeneration phase shows a good agreement with experimental data for the power and the energy consumption even though the simulated values are a bit underestimated, about 10%. The water production is simulated to be about 25% higher than the measured values. This discrepancy could be explained by a leakage of water vapour that was found in the experimental set up, which is not considered in the model. This could also explain the underestimated energy consumption since the condensation energy in the system is too great. To improve the accuracy for the model the water leakage would need to be implemented. The overestimation of water seemed to be the same for the measurements from the same apparatus.

For the adsorption phase a developed model, from an article for adsorption in silica, was implemented and tuned for the specific system. The simulations are in good agreement with the measurements but could be tested further for more certainty.

Handledare: Fredrik Edström
Ämnesgranskare: Per Lötstedt
Examinator: Tomas Nyberg
ISSN: 1401-5757, UPTEC F13 037

Contents

Nomenclature

$\dot{\varepsilon}_w$	Water volume fraction of the cell control volume
$\dot{r}$	Rate of mass transfer between hygroscopic material and surrounding air. $[\frac{kg}{m^3 s}]$
ϵ_β	Volume fraction in the liquid phase
ϵ_γ	Volume fraction in the gaseous phase
ϵ_σ	Volume fraction in the solid phase
Ω_w	Change of volume of liquid water per unit density of moisture $[\frac{m^3}{kg}]$
ρ	Density of material, $[\frac{kg}{m^3}]$
σ	Stefan–Boltzmann constant, the constant of proportionality in Stefan–Boltzmann's law. $\sigma \approx 5.670373 \cdot 10^{-8}$
c_p	Specific heat of material, $[\frac{J}{kgK}]$
D_v	Binary vapour mass diffusion coefficient of water and air mixture
dl_c	The length of the side in a control volume cell that forms a normal to the convecting/radiating area [m]
dL_Y	Length of symmetric segment,[m]
dV_c	The volume of the control volume $[m^3]$
e	The error signal in the PID regulation.
G_γ	The mass flux per second $[\frac{kg}{m^2 s}]$
J_d	Chilton–Colburn mass factor, dimensionless number that approximates the increase in mass transfer
k	Thermal conductivity of material, $[\frac{W}{m^2 K}]$
K_d	The derivative coefficient in the PID regulation.
K_i	The integral coefficient in the PID regulation.
K_p	The proportional coefficient in the PID regulation.
L_X	Width of apparatus,[m]
L_Y	Length of apparatus,[m]
L_Z	Height of apparatus,[m]
M_a	The air molar mass number, $[\frac{g}{mol}]$
Nu	Nusselt number in an enclosure. Dimensionless number that gives a ratio between the convective heat and the conducting heat
Pr	Prandtls number, Dimensionless number that gives a ratio between the viscous diffusion and the thermal diffusion
Ra	Rayleighs numbers, Dimensionless number that is associated with buoyancy driven flow
S_p	The regulation signal, in this case the power signal.
Sc	Schmidt number, Dimensionless number that gives a ratio between the viscous diffusion rate and the mass diffusion rate
Sh	Sherwood number, Dimensionless number that gives a ratio between the convective mass transfer and the diffusive mass transfer
T	Temperature of material
t	Time variable
$T_{current}$	The measured temperature in the PID regulation.
T_{reg}	The wanted temperature in the PID regulation.
U_D	The Darcy velocity, $[\frac{m}{s}]$
V_ρ	Water vapour density in air-vapour mixture, $[\frac{kg}{m^3}]$

1 Introduction

1.1 Background

There are several reason why humidity needs to be controlled. This could be to prevent corrosion, mould growth, health issues and reduced performance in hygroscopic materials like building material.

Corrosion is the slow destruction of materials which often occurs by oxidation of the surface. The phenomenon occurs when the material reacts with oxygen and happens for example when water gets in contact with metallic surfaces. Thus the corrosion depends on the condensed water on the surface. In theory no net condensation of water would occur in an environment under 100% relative humidity (RH). In practice the corrosion can occur at lower RH, since a gradient layer can exist close to surfaces and the rate of condensation and evaporation depends on the relative humidity, making more water molecules available at the surface for interactions. A critical limit exists, where the oxidation rate is significantly lower. For common materials such as iron, steel, zinc and copper, the critical limit of corrosion is between 50-70%. The critical humidity in which mould growth occurs depends on the temperature and on the materials used. This critical limit is for materials higher than 70% relative humidity in 20 degrees and higher in lower temperatures. By lowering the humidity to less than 70% the risk of mould thus is reduced to almost zero [1].

Different types of dehumidification methods exist and the most common are described here.

1.1.1 Heat pump

The heat pump method works by creating a cool and a hot surface by using a compressor and a expansion valve. The air is then flown past the cool surface where the air is cooled. Cool air is less capable of holding water and when the dew point is reached, water condenses on the cool surface. The cooled air then has a relative humidity of 100%. Therefore, the air is reheated with help of the hot surface and the relative humidity decreases to a lower value than the original.

1.1.2 Sorption

In this method, air flows through a hygroscopic material which has a high adsorption capability (in the scale of 30-60% of it's dry weight). The air that should be dehumidified is then passed through the material where water is adsorbed and the dry air is led back into the system. When the material is full of water it cannot any longer adsorb water and thus needs to be regenerated. To do this, warm air is flown through the wet material and this warm high humidity air is led out of the system. This can be done by using a rotating wheel with hygroscopic material divided into a dehumidification section and a regeneration section which rotates the material between the two airflows. This process then becomes continuous.

1.1.3 Controlled Moisture Capture and Release (CMCR)

The CMCR-method is a type of sorption method and it uses hygroscopic material's ability to adsorb water combined with air's inability to hold an infinite amount of water in a closed vessel.

The CMCR method is divided into two phases, the moisture absorption phase and the condensation phase. In the moisture adsorption phase, air is led through the hygroscopic material where it deposits some of its water and thus becomes dehumidified. When the hygroscopic material is full, the airflow stops and the captured water can be condensed by heating it in a closed volume. This makes the air over saturated and forces the water to condensate on the inside of the volume.

1.2 Research on related subjects

A lot of research has been made to create better heat pump and sorption systems. A few example is found, in Choi et al [2], where the steady state and transient performance of a multi-type heat pump system is studied. Equations are presented for the energy, momentum and the continuity of mass. The system is then solved numerically in 1-D using the finite volume method. Tarnawski [3] considers the effects of snow and ice on the performance of a residential heat pump. Ruivo et al [4] investigates a new approach for the effectiveness method to simplify the simulation of desiccant wheels with variable inlet states and airflow rates. Antonellis et al [5] simulates the process of a desiccant wheel dehumidification in order to study the performance and to optimize it with respect to working conditions and revolution speed of the wheel. Enteria et al [6] evaluates the performance of a desiccant wheel experimentally.

In this context this work presents a model to simulate the performance of the novel CMCR sorption method in order optimize the method and to predict the result in different environments. Peng et al [7] and Sun et al present a model for adsorption of water in hygroscopic materials in 1-D, this model was found to be interesting for the modelling of the adsorption phase of the CMCR method.

1.3 Project description

The main objective with this project was to understand the CMCR process and to try to create a tool that can be used in future development of the method. This should be done by developing a model of the system using basic equations and models and see how well the CMCR model could reproduce measured results in the different phases.

1.3.1 Concrete objectives

Concrete objectives for the project where the following:

- Develop and implement a model for the regeneration phase of the CMCR process.

- Implement a model for the adsorption phase of the CMCR process.
- Find software/library to implement the models to be solved numerically
- Make measurements of the temperature, power, energy and water production of the regeneration phase of the process.
- Make measurements of the temperature and relative humidities during the adsorption phase of the process.
- Make measurements of adsorption capabilities of the hygroscopic materials.
- Implement the model and compare and validate with data from the measurements.

1.3.2 Purpose

When creating this model the objective was to understand the process of the CMCR method and see how well the process could be reproduced using basic models describing the different phases. This gives more insight in which parts that are important for the process and how this can be used. By knowing more about the system, problems can be foreseen and new improvements can be found. Creating and designing new prototypes can be a costly procedure and often require a lot of effort when testing new concepts. By creating a model of a system, a lot of different designs and concepts can be evaluated before building an expensive prototype.

If the model is satisfactory the environmental differences, i.e. different ambient temperatures and humidities can be investigated or different hygroscopic materials or regulations methods can be tested.

2 Theory of the Modeling of CMCR method

In this section the theory and equations needed for the thesis are described. The properties of hygroscopic materials are presented in more detail. The CMCR-system is described further. Both the regeneration and adsorption phase are described closer and the equations for how to model the two phases are presented.

2.1 Hygroscopic Materials

A hygroscopic material is a material that has the capability to adsorb a high amount water, in the range up to 70% of its dry mass weight. With adsorption means that the adsorbate (water in this case) binds to the surface of the adsorbent. The type of binding that this is done with can depend on which material and species that are involved. Typically the bindings is made of weak van der Waal bindings or covalent bindings [8]. Adsorption is a surface phenomenon and the performance of a hygroscopic material depends on the properties and area of the surface. This is not to be confused with absorption which is a volume phenomenon where the absorbate is dissolved into the absorbent.

The hygroscopic property of the material can be measured by creating an adsorption curve where the amount of adsorbed water is noted for different humidity levels. These adsorption curves depends on the porosity of the material, how much surface there is for the adsorbate to bind to, how big the pores/cavities are etcetera. If the cavities are big then they cannot adsorb much water when the surrounding relative vapour pressure is low, that is a low relative humidity. On the contrary, when the humidity is close to the saturation value, the adsorbent can adsorb a lot of water. Hygroscopic materials with narrow pores can adsorb water at low humidities but can instead not adsorb as much water as the wide pore desiccant at higher humidity levels.

Typical hygroscopic materials are wood, silica gel, zeolites and activated aluminium. In this report mostly silica gel used but also activated aluminium.

2.1.1 Silica gel

Silica gel (SiO_2) has been used for the last two decades as a desiccant, its high performance adsorption capability makes it very suitable to remove water vapour from systems. The great adsorption capacity of silica gel comes from the micro porous structure consisting of interlocking cavities. These cavities give the silica gel a high internal surface for the water to bind to (up to $800\frac{m^2}{g}$) [9].

As described before, the water vapour in the adjacent air diffuses into the internal cavities of the material if the vapour pressure is lower than the surrounding vapour pressure. The higher the humidity is the more water will be able to adhere on the surface. The adhering on the surface does not create a chemical reaction and the particles do not change in shape or appearance. The adsorption curve may differ between manufacturers due to different methods of production [10].

The adsorption curve for the material that is used in this report is not known and thus needs to be investigated. Silica gel also has the ability to be regenerated, that is by increasing the temperature of the silica, the vapour pressure is increased and the water evaporates from the surface. Even though silica gel has been used for a long time the heat and transfer process inside the pores are still being researched.

2.2 The CMCR-system

The system consists mainly of a heating device, hygroscopic material, air and an enclosure. During the adsorption phase, the hygroscopic material adsorbs water vapour from the flowing air. This proceeds until the hygroscopic material is saturated and thus needs to be regenerated. This regeneration process works by sealing the enclosure and then heat the system. By doing this the vapour pressure inside the hygroscopic particles is increased and as a consequence, water vapour is released from the particles. Since the surrounding air only can hold a certain amount of water, this leads to an oversaturation of the air and the water condenses inside the enclosure and the water can be led out from the system.

2.3 Modelling the regeneration phase

In this project, a model of the regeneration phase has been created using a combination of physical models. To lower the complexity of the problem, the problem was reduced from 3-D to 2-D. To compensate for this simplification and to still be able to simulate the system, scale factors for the heat and mass transfer were introduced. These are the Nusselt and Sherwood numbers, which are described in more detail below. The geometry of the model can be seen in Figure 1.

The geometry is seen as a cut through the plane of the apparatus with the vertical axis as normal. The geometry consists of an inner frame which contains a bed of hygroscopic particles. Inside the bed a radiator with fins is located. The frame is then located inside an enclosure and between the frame and the enclosure wall an gap is created. The geometry is only describing one side of the apparatus, since symmetry can be used.

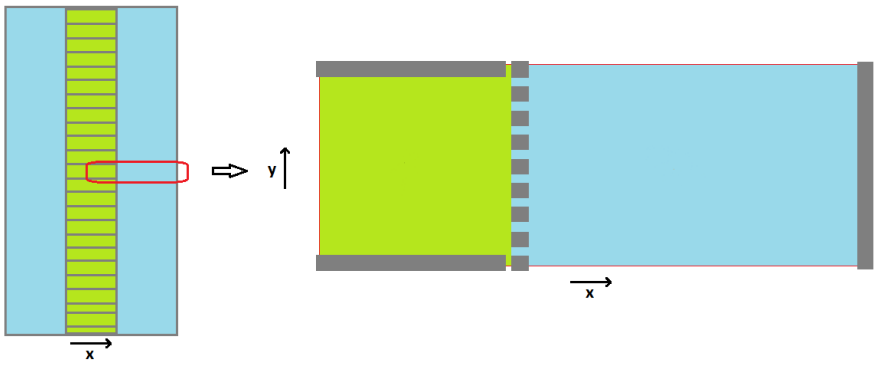

Figure 1: The geometry of the modelling system, shown as a cut through a plane with the z-axis as normal. (1) The bed of hygroscopic material, (2) a radiator fin for heating power, (3) the frame holding the bed, (4) symmetry axis, (5) air gap between frame and enclosure and (6) the enclosure wall, facing the ambient temperature.

On this geometry an orthogonal mesh was created. The different parts of the mesh were then given different physical properties, i.e. specific heat, density and thermal conductivity.

To model the heat transport in the material, a diffusion equation is implemented for both solid and gaseous materials. The bed with hygroscopic material is homogenised by letting the physical properties of the materials be weighted by their masses. The bed is also assumed to be in thermal equilibrium with the gas surrounding the material. An energy source is introduced to the system to model the heating from the radiator fins. The energy input can be controlled by letting the system be regulated by a PID-controller.

In the model the total pressure of the gas is held at constant atmospheric pressure. This implies that there is no bulk motion out from the system. Since the frame creates a cold and a hot surface, a bulk movement of air is created within the system. The density of air is lowered when heated and thus air rises on the inside of the frame and then falls down when cooled by the enclosure. This creates a rotation which increases both the mass and heat transport of the system. This rotation is occurring orthogonal to the modelling plane and to avoid the need of a 3D-model, the rotating phenomenon is taking into account by scaling the heat and mass transfer through the air gap.

The advection within the enclosed air gap can be model by scaling the thermal conductivity by the Nusselt number for an enclosed vessel [11]. This relation is valid for steady state and not necessarily during the transient phase. The time for the boundary layer in the enclosure to reach equilibrium can be approximated by using equations from Faghri [12]. The time scale for this movement is about one second, which is a short time in this model. As for the thermal diffusion, the advective vapour mass transport is modelled by using the Sherwood number, which is the equivalent of the Nusselt number for mass transport. As with the

Nusselt number the Sherwood number is used to scale the diffusion coefficient due to the circular motion created inside the enclosure. If an expression for the Nusselt number is known, the Sherwood number can be approximated by substituting the Prandtl number with the Schmidt number in this equation. That is, if $Nu = f(Pr, Re)$ then $Sh \approx f(Sc, Re)$, where Nu is the Nusselt number, Pr the Prandtl number, Re the Reynolds number, Sc the Schmidt number and Sh the Sherwood number [13].

Energy is also transported from the inner frame to the enclosure by radiation since there is a notable difference in temperatures on the different sides of the air gap. On the outside of the enclosure, energy can dissipate by both convection and radiation. Depending on the ambient environment the convection can be either natural or forced.

The transport of water is modelled as diffusion in the gaseous phase since the total pressure is held at atmospheric pressure and there is therefore no bulk motion of the gas apparent. The water in the liquid phase is considered immovable since the water is contained in particles which are separated by air. The water inside the particles can diffuse within the particles but no further and the transport is therefore modelled by water evaporating from the surface of the particles and from there diffusing as vapour out from the hygroscopic bed. The evaporation transport of water from within the particle to the air vapour gas mixture is modelled with the difference in vapour pressure as the driving force as in [7] and [14]. The water can then be adsorbed again in an other particle if the water content there is low enough. When the water is evaporated in the hygroscopic material, energy is taken from the surrounding material to exceed both the energy of vaporisation and the binding energy holding the water at the surface. This is modelled as a sink or a source in the hygroscopic material depending on if the water is adsorbed or desorbed.

To model the condensation of water, the water is said to condense on the inside of the enclosure when the amount of water in the vapour creates a partial pressure higher than the saturation vapour pressure. The difference in vapour pressure is recalculated as a difference in mass using the ideal gas law. If the vapour mass is higher than the saturation vapour mass the the difference is removed from the system. The condensation on the enclosure also releases energy to the surrounding material as the water changes phase. This is modelled as a source on the inner surface of the enclosure.

2.3.1 Assumptions made when modelling the regeneration phase

(1) The air and vapour inside the bed and in the air gap are assumed to be an ideal gas mixture and follow the ideal gas law.

(2) The properties of the particles are homogeneous and isotropic.

(3) The air and vapour mixture surrounding the hygroscopic bed are said to be in thermal equilibrium with the bed at all times.

(4) Water contained within particles cannot move in the bed as liquid, and no dissolution or chemical reactions takes place in the bed.

(5) The pressure is constant equal to atmospheric pressure in the modelling plane. That is, there is no advection present in the plane.

(6) The internal moisture transport between particles and air, depends on the difference in vapour pressure, which is related to the adsorption equilibrium curve.

(7) The equilibrium adsorption curve is constant with temperature.

2.3.2 Governing equations of the regeneration phase

The energy conservation equation for the system in 2D is written as follows,

$$\begin{aligned}\frac{\partial(c_{p-eff}\rho_{eff}T)}{\partial t} &= \nabla\cdot(k_{eff}\nabla T) + \frac{dL_Y W_{in}}{L_Y dV_c} + \dot{r}\lambda_\sigma + \dot{c}\lambda_\beta \\ &- \frac{\sigma\epsilon_{f\to ei}}{dl_c}(T_f^4 - T_{ei}^4) + \frac{\sigma\epsilon_{ei\to f}}{dl_c}(T_f^4 - T_{ei}^4) \\ &- \frac{h_\infty}{dl_c}(T_{eo} - T_\infty) - \frac{\sigma\epsilon_{eo}}{dl_c}(T_{eo}^4 - T_\infty^4).\end{aligned} \tag{1}$$

where the term

$$\nabla\cdot(k_{eff}\nabla T) \tag{2}$$

comes from the thermal diffusion,

$$\frac{dL_Y W_{in}}{L_Y dV_c} \tag{3}$$

represents the energy input to the system,

$$\dot{r}\lambda_\sigma + \dot{c}\lambda_\beta \tag{4}$$

are sources and sinks from the condensation and evaporation of water that occur both on the enclosing wall and in the hygroscopic material. The terms

$$-\frac{\sigma\epsilon_{f\to ei}}{dl_c}(T_f^4 - T_{ei}^4) + \frac{\sigma\epsilon_{ei\to f}}{dl_c}(T_f^4 - T_{ei}^4) - \frac{\sigma\epsilon_{eo}}{dl_c}(T_{eo}^4 - T_\infty^4) \tag{5}$$

are sinks and sources to represent the radiation both out from the system and between the walls in the gap and

$$\frac{h_\infty}{dl_c}(T_{eo} - T_\infty) \tag{6}$$

describes the energy dissipation by convection on the outer wall.

The gas mixture is in thermal equilibrium with the solid and liquid in the hygroscopic material. Therefore the three energy equations describing the energy transport in the solid, the liquid and the gaseous material can be combined

into one. The total pressure is constant equal to the atmospheric pressure in the modelling plane and thus the advective term $\nabla(\vec{\mathbf{u}}T)$ is neglected from the heat transfer equation. The rotating velocity field created in the z-direction perpendicular to the modelling plane is accounted for by scaling the thermal conductivity with the Nusselt number.

In (1), c_{p-eff} is the weighted specific heat, k_{eff} is the weighted thermal conductivity, ρ_{eff} is the weighted density. The weighting is done as follows. The specific heat is

$$c_{p-eff} = \frac{c_{pw}\epsilon_w\rho_w + c_{p\sigma}\epsilon_\sigma\rho_\sigma}{\epsilon_w\rho_w + \epsilon_\sigma\rho_\sigma}, \tag{7}$$

the density is

$$\rho_{eff} = \frac{\epsilon_w\rho_w + \epsilon_\sigma\rho_\sigma}{\epsilon_w + \epsilon_\sigma}, \tag{8}$$

and the thermal conductivity is

$$k_{eff} = \frac{k_w\epsilon_w\rho_w + k_\sigma\epsilon_\sigma\rho_\sigma}{\epsilon_w\rho_w + \epsilon_\sigma\rho_\sigma}. \tag{9}$$

L_Y is the length of the apparatus, dL_Y is the length of a symmetric segment (length of (4) in Figure 1), dl_c is the length of the side in a control volume cell, that forms a normal to the convecting/radiating area. dV_c is the volume of the control volume. $\dot{r}$ is the adsorption/desorption rate, λ_σ is the vapourisation energy in the hygroscopic material, $\dot{c}$ is the condensation rate on the enclosure and λ_β is the vapourisation energy on the surface. Water is said to condense if the amount of vapour in air is higher than the saturation amount. That is

$$\dot{c} = \begin{cases} dV_c(V_p - V_{sat}) & \text{if} \quad V_p > V_{sat} \\ 0 & \text{otherwise} \end{cases} \tag{10}$$

Inside the gap, the thermal conductivity is scaled with the Nusselt number as

$$k_{gap} = k_{eff}Nu, \tag{11}$$

where

$$Nu = 0.42Ra^{\frac{1}{4}}Pr^{0.012}\left(\frac{L_Z}{L_{gap}},\right)^{-0.3}, \tag{12}$$

$$Ra = \frac{g\beta PrL_{gap}^3}{\nu}(T_f - T_{ei}), \tag{13}$$

and

$$Pr = \frac{\mu c_p}{k}. \tag{14}$$

g is the gravitational acceleration, β is the thermal expansion given by $\beta = \frac{1}{T_{f-ie}}$ and ν is the dynamic viscosity.

The mass transfer equation for water vapor is given by

$$\frac{\partial V_\rho}{\partial t} = \dot{r} + \nabla \cdot (D_v \nabla V_\rho). \tag{15}$$

Where V_ρ is the water vapour density and D_v is the binary vapour mass diffusion coefficient of water and air mixture. Also here the advection term $\nabla(\vec{\mathbf{u}}V_\rho)$ is neglected and replaced by a scaling of the vapour diffusion with the Sherwood number inside the air gap as follows,

$$D_v = ShD_{vgap}, \tag{16}$$

where D_{vgap} is given by

$$D_{vgap} = 2.3e^{-5}\frac{p_0}{p}(\frac{T}{273}^{1.81})[15] \tag{17}$$

and

$$Sh = 0.42Ra^{\frac{1}{4}}Sc^{0.012}\left(\frac{L_Z}{L_{gap}}\right)^{-0.3} \tag{18}$$

where

$$Sc = \frac{\mu}{\rho D}. \tag{19}$$

The liquid water conservation equation is given by

$$\frac{\partial \varepsilon_w}{\partial t} = -\Omega_w \dot{r} \tag{20}$$

where ε_w is the water volume fraction of the cell control volume and $\Omega_w = \frac{1}{\rho}$ is the change of volume of liquid water per unit density of moisture. The adsorption/desorption rate has been modelled as proportional to the difference in vapour pressure on the surface of the adsorbent and the vapour pressure in the surrounding air as follows

$$\dot{r} = k_b A_\sigma \left(P_{v\sigma} - P_{va}\right), \tag{21}$$

where k_b is the internal mass transfer coefficient and A_σ is the apparent surface of the hygroscopic material. From the definition of the relative humidity, $RH = \frac{P_v}{P^{''}}$, the vapor pressure could be written as

$$P_{v\sigma} = RHP^{''}(T), \tag{22}$$

where $P^{''}(T)$ is the saturation vapour pressure for that temperature, given by the Wagner equation [16] as follows,

$$ln\left(\frac{P^{''}(T)}{P_c}\right) = \frac{T_c}{T}\left(a_1\tau + a_2\tau^{1.5} + a_3\tau^3 + a_4\tau^{3.5} + a_5\tau^4 + a_6\tau^{7.5}\right) \tag{23}$$

with

$$
\begin{array}{ll}
a_1 = -7.85951783 & a_4 = 22.6807411 \\
a_2 = 1.84408259 & a_5 = -15.9618719 \\
a_3 = -11.7866497 & a_6 = 1.80122502 \\
T_c = 647.096K & P_c = 22.064MPa \\
\theta = \frac{T}{T_c} & \tau = 1 - \theta.
\end{array}
$$

The relative humidity can then be related to the water content by creating an equilibrium adsorption curve for the specific material as follows

$$RH = \phi(X). \tag{24}$$

This equation describes the equilibrium water content in the material for different relative humidity environments. How this curve is obtained is described in Section 3.4. The curve is fitted by a second degree polynomial with a zero constant term. The fitted function for silica is given by

$$\phi(X) = 2.665X^2 + 0.955X \tag{25}$$

and for activated alumina it is given by

$$\phi(X) = -3.7495X^2 + 3.8711X \tag{26}$$

Combining (22) and 24 gives the relation

$$P_{v\sigma} = \phi(X)P(T), \tag{27}$$

which inserted into Equation (21) gives

$$\dot{r} = k_b A_s \left(P_{va} - \phi(X)P_{vs\sigma}\right). \tag{28}$$

This approach is used in Peng et al[7], Sun and Besant[14] and Rady et al[17].

2.3.3 PID regulation

To control the system behaviour and to be able to maintain a certain temperature in the system, a PID regulation was used. This PID regulation was also implemented in the model. The PID regulation uses a proportional, an integral and a derivative term with the error signal to adjust the input. That is

$$S_p = K_p e + K_i \int e dt + K_d \frac{de}{dt} \tag{29}$$

where S_p is the regulation signal, K_p is the constant in the proportional term, K_i the integral term constant, K_d the derivative term constant and e is the error signal ($e = T_{current} - T_{reg}$). If the system to be controlled has a limit in the regulation, that is the input signal is limited and cannot always be as high as the regulation signal requests, the regulation can become very poor. If the integral term becomes too large because the system reacts slower than expected from the PID, then this creates an overshoot on the system. To avoid this, the integral term is not integrated until the output signal is lower than the threshold. This is also implemented in the model. The PID regulation is made on the mean value on a square segment in the middle of the frame during the simulation to be as similar to the real system as possible.

2.4 Modelling of adsorption phase

When the apparatus is in the adsorption phase, air is blown with help of a fan through the bed with hygroscopic particles. The flow is assumed to be isotropic and homogeneous and the bed thickness,L_x, is assumed to be constant over the whole bed. This makes it possible to approximate the system by a 1-D model. The model of the adsorption phase is as in the regeneration phase created by a combination of heat and mass transfer models. There is no external source during the adsorption phase but heat is transferred to the system when water vapour is adsorbed and releases its heat of vapourisation to the surrounding material. The heat is transferred and dissipated by diffusion in both the gaseous and the solid phases and also by advection in the gaseous phase where heat is transferred by the moving air. The liquid water is said to be immovable in the particles, i.e. the water can not diffuse in liquid form through the bed. The water vapour is transferred by both diffusion and advection in the gaseous phase. The transfer rate of water vapour between the gas and the particles is proportional to the difference in vapour pressure.

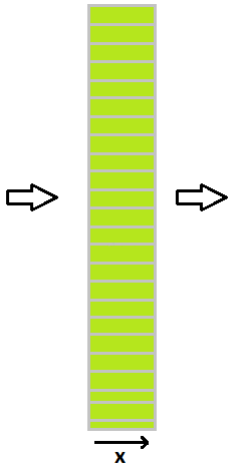

Figure 2: The geometry of the modelling system in the adsorption phase. (1) The inlet after the fan and before the hygroscopic bed, (2) the hygroscopic bed and (3) the outlet.

2.4.1 Assumptions made when modelling the adsorption phase

(1) The air and vapour inside the bed are assumed to be an ideal gas mixture and following the ideal gas law. The air and vapour mixture has a unique temperature at any point; the solid hygroscopic material and the adsorbed water are assumed to be in thermal equilibrium and is not necessarily equal to the temperature of the gaseous phase.

(2) The properties of the particles are homogeneous and isotropic.

(3) Water contained within particles cannot move in the bed as liquid, and no dissolution or chemical reactions takes place in the bed.

(4) The flow is homogeneous and isotropic over and through the bed.

(5) The internal moisture transport between particles and air, depends on the difference in vapour pressure, which is related to the adsorption equilibrium curve.

(6) The equilibrium adsorption curve is constant with temperature.

2.4.2 Governing equations of the adsorption phase

The energy conservation equation for the gaseous phase is written as follows,

$$\frac{\partial(\epsilon_\gamma c_{p\gamma}\rho_\gamma T_\gamma)}{\partial t} + \nabla(\vec{U}_D \rho_\gamma c_{pa} T_\gamma) = \nabla \cdot (\epsilon_\gamma k_{\gamma,eff} \nabla T_\gamma) + h_{\sigma\gamma} A_\sigma (T_\gamma - T_\sigma) \quad (30)$$

where the term

$$\nabla \cdot (\epsilon_\gamma k_{\gamma,eff} \nabla T_\gamma) \quad (31)$$

represents the diffusion, the term

$$\nabla(\vec{U}_D \rho_\gamma c_{pa} T_\gamma) \quad (32)$$

the advection and the term

$$h_{\sigma\gamma} A_\sigma (T_\gamma - T_\sigma) \quad (33)$$

the energy transfer between the solid and the gaseous phase.

The energy equation for the solid and liquid phase is written as follows.

$$\frac{\partial(\epsilon_{\sigma\beta} c_{p\sigma\beta}\rho_{\sigma\beta} T_{\sigma\beta})}{\partial t} = \nabla \cdot (\epsilon_{\sigma\beta} k_{\sigma\beta,eff} \nabla T_{\sigma\beta}) - h_{\sigma\gamma} A_\sigma (T_\gamma - T_{\sigma\beta}) + \dot{r}\lambda \quad (34)$$

where the term

$$\nabla \cdot (\epsilon_{\sigma\beta} k_{\sigma\beta,eff} \nabla T_{\sigma\beta}) \quad (35)$$

represents the diffusion, the term

$$-h_{\sigma\gamma} A_\sigma (T_\gamma - T_{\sigma\beta}) \quad (36)$$

the energy transfer between the gaseous and solid phase and the term

$$\dot{r}\lambda \quad (37)$$

the energy from the evaporation and condensation in the hygroscopic material.

The solid and liquid phase are said to be in thermal equilibrium and can thus be treated with one energy equation. The energy transfer between the solid/liquid phase and gas phase is proportional to the difference in temperature

and the proportionality constant depends on the apparent area between the phases times the convective constant. The physical properties of both the gas mixture and the solid liquid mixture are mixed by mass as done in Equation (7) - (9).

The internal mass transfer,k_b in (28) can according to Peng et al [7] be approximated by the relation

$$k_b = \frac{J_d G_\gamma}{M_a P_a S c^{\frac{2}{3}}} \tag{38}$$

where G_γ is the mass flux per second, J_d is the Chilton–Colburn mass factor,M_a is the air molar mass number, P_a is the air partial pressure and Sc the Schmidt number. The mass flux is determined from

$$G_\gamma = \frac{U_D \rho_\gamma}{\epsilon_\gamma} \tag{39}$$

where ϵ_γ is the volume fraction in the gaseous phase and U_D is the Darcy velocity. The Chilton–Colburn mass factor, J_d is given by

$$J_d = 0.048 Re^{-03} \tag{40}$$

where the Reynolds number, Re, is given by

$$Re = \frac{4 r_h G_\gamma}{\mu}. \tag{41}$$

μ is the dynamic viscosity and r_h is the hydraulic radius given by

$$r_h = \frac{\epsilon_\gamma}{A_\sigma}. \tag{42}$$

The adsorption curve $\phi(X)$, is given by (25) and (26). The water content, X, is there given by

$$X = \frac{\epsilon_\beta \rho_\beta}{\epsilon_\sigma \rho_\sigma}. \tag{43}$$

ϵ_β is the volume fraction of liquid water and ϵ_σ is the volume fraction of solid. The convective heat transfer constant, $h_\sigma \gamma$ is approximated with help of the Chilton-Colburn heat transfer factor as

$$h_\sigma \gamma = \frac{J_h c_{pa} G_\gamma}{Pr^{\frac{2}{3}}}, \tag{44}$$

where

$$J_h = 0.052 Re^{-0.3}. \tag{45}$$

The water vapour mass transfer equation is given by

$$\frac{\partial \epsilon_\gamma V_\rho}{\partial t} + \nabla(\vec{U}_D V_\rho) = \nabla \cdot (\frac{\epsilon_\gamma D_v}{\tau} \nabla V_\rho) - \dot{r}. \tag{46}$$

The difference from the vapour density transport equation in the regeneration phase given by (15) is that the advection term cannot be neglected here and that the diffusion is scaled by the tortuosity,τ. According to Punčochář[18] the tortuoisity is related to the porosity by

$$\tau = \frac{1}{\sqrt{\epsilon_\sigma}}. \tag{47}$$

The liquid water conservation equation is given as (20) in the regeneration phase by

$$\frac{\partial \varepsilon_w}{\partial t} = -\Omega_w \dot{r}. \tag{48}$$

From Darcy's momentum equation

$$U_D = -\frac{K}{\mu}\frac{dP}{dx}, \tag{49}$$

the pressure drop through the bed can be calculated by knowing the Darcy velocity. The pressure drop is then calculated as

$$P(x) = P_\infty + \frac{U_D \mu}{K}(L_X - x), \tag{50}$$

where L_X is the thickness of the hygroscopic bed.

By using the ideal gas law, the partial vapour pressure and the gas density can be calculated from the following relationships

$$P_v = \frac{V_\rho R T_\gamma}{M_a}, \tag{51}$$

$$P_a = P(x) - P_v, \tag{52}$$

$$\rho_a = \frac{P_a M_a}{R T_\gamma} \tag{53}$$

and

$$\rho_\gamma = \rho_a + V_\rho. \tag{54}$$

The bed is initially considered to have an uniform temperature distribution and water content. That is

$$t = 0: \qquad T_\gamma = T_\sigma = T_0 \tag{55}$$

and

$$t = 0: \qquad V_\rho = V_{\rho 0}, X = X_0 \tag{56}$$

The inlet conditions are given by

$$x = 0: \qquad T_\gamma = T_\infty, \frac{\partial T_\sigma}{\partial x} = 0, V_\rho = V_{\rho\infty} \tag{57}$$

and the outlet conditions are given by

$$x = L_x: \qquad \frac{\partial T_\gamma}{\partial x} = 0, \frac{\partial T_\sigma}{\partial x} = 0, \frac{\partial V_\rho}{\partial x} = 0 \tag{58}$$

3 Method

3.1 Numerical method and programming

Different applications and frameworks were investigated as tools to discretise and solve the equations given in Section 2. The tool should have functionality to implement the equations fairly easy and to visualise the result. Since the project had a limited funding, tools like Comsol Multiphysics and Autodesk couldn't be used. The tool chosen was a programming framework written for python, FiPy [19]. This is a free library developed by the Materials Science and Engineering Division (MSED) and Center for Theoretical and Computational Materials Science (CTCMS), in the Material Measurement Laboratory (MML) at the National Institute of Standards and Technology (NIST). With this python library the equations could be discretised on a given geometry using the finite volume method.

3.1.1 Regeneration phase

First the geometry had to be defined and since the geometry that was chosen was easy to represent by squares, an orthogonal grid were used, see Figure 1. Solution variables were then defined on this grid, the temperature T, the amount of water in the hygroscopic material W and the vapour content in air V. Variables for the density, specific heat, thermal conductivity, emissivity and diffusion were also defined on the grid. From these variables, the vapour pressure, saturation pressure, the water transmission rate, convection and radiation terms could be calculated, following the equations in Section 2.3.2. The boundary conditions for the top, bottom and left side of the segment were symmetric and were given by zero flux across the symmetry plane, that is zero gradients at $y = 0$, $y = L_y$ and $x = 0$. At $x = L_x$ the boundary was a convection and radiation boundary. The internal boundary conditions with radiation between the frame and the wall were treated as a source term applied in the first segment of the wall. This was necessary since FiPy didn't have a way to treat this. The PDE system in (1) was implemented using classes from the FiPy library that represented diffusive terms, transient terms and convection terms including the solution variables. The terms could either be solved implicitly or explicitly depending on the problem. Although more calculations are needed with an implicit scheme, it was still preferred to be able to get a stable solution at longer time steps. A loop was then created in the program where the equations where solved for each time step. Since the equations are coupled, the solution was iterated until convergence. Convergence was obtained when the solution had changed less than $10e^{-5}$ from the last sweep. When convergence was reached, the solution variables were updated and vapour pressures, diffusion, regulation parameters, convection, radiation, changes in physical properties of air etcetera, were recalculated to be used in the next time step. This was then repeated until the simulation end time had been achieved. The time step was chosen to be 2.5 seconds, since very small changes were found from changing between 5, 2.5 and

1 seconds. The conservation of mass and energy was also investigated during the simulation and conservation of mass was found to change less than 0.01% comparing to the start value. The energy conservation was less good, and had a conservation about 1%, this was on the other hand harder to measure since the total energy input should be compared to the total energy of the system at all points. This can be seen in Figure 3 and 4. Since some energy where incorporated in the evaporation of water and then returned as when condensed, it was complicated to get the total energy calculated in an accurate. The input energy was also calculated by a simple trapezoidal integration which contributes to the low accuracy.

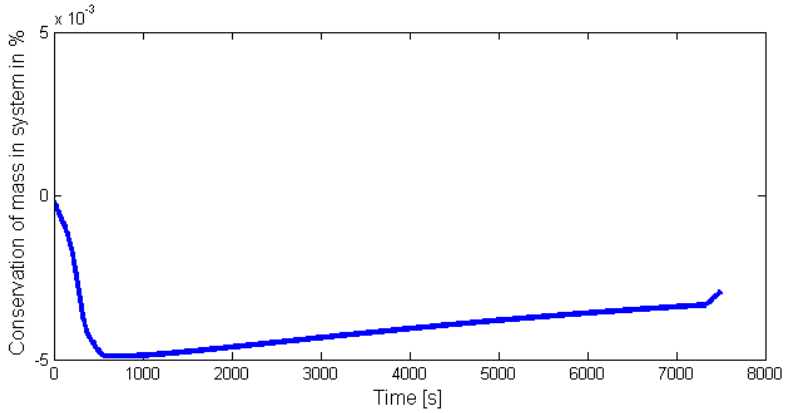

Figure 3: The conservation in mass measured in % of the original value of the system mass.

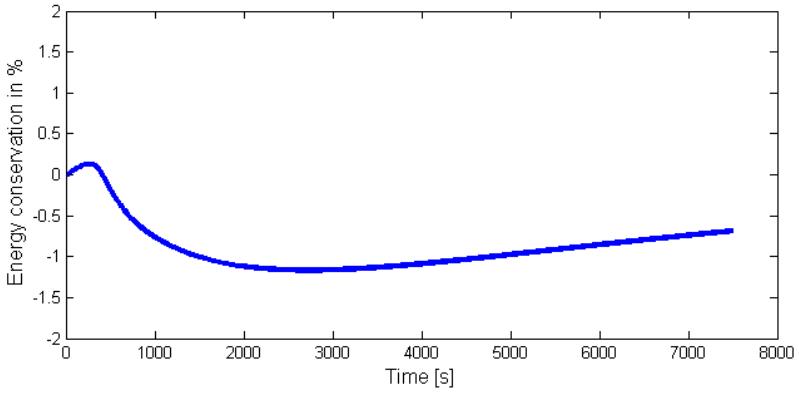

Figure 4: The conservation of energy measured in %. The integrated input power compared to the energy stored in the system at a specific time.

3.1.2 Adsorption phase

The geometry here was simpler and thus only required a 1-dimensional grid. Also here solution variables were created, variables for the temperature of the gas T_γ, the temperature of the solid hygroscopic material and the liquid, T_σ, the water content of the hygroscopic material W and the water vapour content in the air V. From Darcy's law the pressure in the bed could be calculated according to (50). The saturation pressure could for each time step be calculated from (23). The vapour pressure and density for the gas were then calculated using (51)-(54). The PDE given by (30), (34), (46) and (48) were implemented using implicit solvers for the transient, diffusion and convection terms from the FiPy library. Since the convection term is dominating the solution of the gas equations, an upwind convection term was used. The solution was iterated also for these equations. The convergence was defined as before to be achieved when the solution for each time step had changed less than 10^{-5}. When convergence was obtained, the solution variables were updated and used to recalculate vapour pressure, the water transmission rate and other properties used for the next time step.

The simulation of the adsorption phase was compared to a test where the frame was filled with almost dry silica gel. The mass and the parameters used for the adsorption phase are shown in Table 4. The Colburn heat and mass transfer number were adjusted for the simulation to fit the measured data better.

3.2 Test cases for comparing with simulations

The simulation of the regeneration phase was compared in three test cases. One case where the regulation temperature was held at a constant of 100 degrees Celsius. This is referred to as Case 1. In Case 2 the regulation temperature was changed first from 110 degrees to 120 degrees and then to 140 degrees. This was done after 4000 and 5850 seconds respectively. The last test (Case 3) was conducted on a smaller prototype where the maximum input power was lower and the temperature was set to a constant of 135 degrees Celsius. The shape of the prototype was different and it used different regulation constants. Since the water transmission coefficient was unknown, k_b in (28), for the simulation it was fitted so that the water loss in the hygroscopic material matched the water loss of the frame in the measured test cases. Some of the parameters used when calculating the regeneration phase are shown in Table 1, 2 and 3. The materials and exact geometry are not included.

Table 1: Parameters used when modelling the regeneration phase of the CMCR system for Case 1 with constant regulation temperature of 100 degrees Celsius

$d_s = 2 \cdot 10^{-3} m$	$P_{atm} = 101325 Pa$
$\rho_s = 2200 \frac{kg}{m^3}$	$T_{amb} = T_0 = 25 C$
$\rho_{sbulk} = 790 \frac{kg}{m^3}$	$T_{reg} = 100 C$
$c_{ps} = 1000 \frac{J}{kgK}$	$m_{sdry} = 4380 g$
$k_{effs} = 0.19 \frac{W}{mK}$	$RH_0 = 43\%$
$\phi(X) = 2.665X^2 + 0.955X$	$X_0 = 27.8\%$
$S_v = 600 \frac{m^2}{g}$	$W_{max} = 2220 W$
$k_b = 2.5 \cdot 10^{-8}$	$K_p = 65$
$\lambda_h = 2420000 \frac{J}{kg}$	$K_I = 0.045$
$t_{end} = 7500 s$	$K_D = 1000$

Table 2: Parameters used when modelling the regeneration phase of the CMCR system for Case 2, with step wise changed regulation temperature.

$d_s = 2 \cdot 10^{-3} m$	$P_{atm} = 101325 Pa$
$\rho_s = 2200 \frac{kg}{m^3}$	$T_{amb} = T_0 = 25 C$
$\rho_{sbulk} = 790 \frac{kg}{m^3}$	$T_{reg} = 110, 120, 140 C$
$c_{ps} = 1000 \frac{J}{kgK}$	$m_{sdry} = 6080 g$
$k_{effs} = 0.19 \frac{W}{mK}$	$RH_0 = 40\%$
$\phi(X) = 2.665X^2 + 0.955X$	$X_0 = 26.0\%$
$S_v = 600 \frac{m^2}{g}$	$W_{max} = 2220 W$
$k_b = 2.52 \cdot 10^{-8}$	$K_p = 65$
$\lambda_h = 2420000 \frac{J}{kg}$	$K_I = 0.045$
$t_{end} = 7200 s$	$K_D = 1000$

Table 3: Parameters used when modelling the regeneration phase of the CMCR system for Case 3, a smaller system.

$d_s = 2 \cdot 10^{-3} m$	$P_{atm} = 101325 Pa$
$\rho_s = 2200 \frac{kg}{m^3}$	$T_{amb} = T_0 = 25 C$
$\rho_{sbulk} = 860 \frac{kg}{m^3}$	$T_{reg} = 130 C$
$c_{ps} = 1000 \frac{J}{kgK}$	$m_{sdry} = 1.280 g$
$k_{effs} = 0.19 \frac{W}{mK}$	$RH_0 = 65\%$
$\phi(X) = 2.665X^2 + 0.955X$	$X_0 = 35.0\%$
$S_v = 600 \frac{m^2}{g}$	$W_{max} = 612 W$
$k_b = 2.5 \cdot 10^{-8}$	$K_p = 10$
$\lambda_h = 2420000 \frac{J}{kg}$	$K_I = 0.0877$
$t_{end} = 2725 s$	$K_D = 0$

Table 4: Parameters used when modeling the adsorption phase of the CMCR system.

$d_s = 2 \cdot 10^{-3} mm$	$P_{atm} = 101325 Pa$
$\rho_s = 2200 \frac{kg}{m^3}$	$k_\sigma = 0.11$
$\rho_{sbulk} = 790 \frac{kg}{m^3}$	$k_\beta = 0.58$
$c_{ps} = 1000 \frac{J}{kgK}$	$k_{vapor} = 0.026$
$k_{effs} = 0.19 \frac{W}{mK}$	$RH_0 = 38\%$
$\phi(X) = 2.665X^2 + 0.955X$	$X_0 = 4.5\%$
$S_v = 15000 \frac{m^2}{m^3}$	$t_{end} = 14000 s$
$\lambda_h = 2420000 \frac{J}{kg}$	$U_D = 0.45$

3.3 Experimental setup for test cases

The simulations were compared to different test cases. Before the regeneration phase, the hygroscopic material in the frame was saturated in a known environment, the weight of the frame was measured so that the transmission rate coefficient could be fitted and the water content was also measured by weighing a sample of the hygroscopic material. During the test, the ambient temperature, the temperature in the hygroscopic material, the requested input energy, the real used energy and the water production were logged. The result from these comparisons can be seen in Section 4.1. When conducting the measurement of the adsorption phase a frame with as dry silica gel as possible was prepared. The water content was measured to approximately 4.5%. The temperature and relative humidity were logged for both the inlet, the outlet and the temperature inside the frame of hygroscopic material. The mass flow into the system was also needed. This was measured by using a special pipe where the pressure drop was measured. This pressure drop then corresponded to an air flow through the pipe. To complement this, the air speed was measured in the pipe and an approximation of the air flow through this pipe was made. The flow was approximated to $290 \frac{m^3}{hour}$ with an error estimated to $\pm 5\%$. The relative humidity sensors had a bias of $\pm 2\%$ and the temperature sensors have an error less than 0.5%.

3.4 Measurement of Adsorption curves

The equilibrium adsorption curves of silica gel and activated aluminum needed to been determined experimentally. This was done by creating controlled environments for different relative humidities. To get good characteristics of the adsorption curves, five humidity points were chosen. For best result these points were evenly distributed over the relative humidity spectra, giving points at about 20% RH, 40% RH, 60% RH, 80% RH and 100% RH.

To be able to create controlled environments, saturated salt solutions were used. When containing salt solutions in a closed volume with surrounding air, an equilibrium humidity is obtained. Depending on the type of salt and the amount

of salt, different equilibria can be achieved. The equilibrium is maintained as long as the amount of salt in the water-salt solution is over the maximum solubility of the specific salt. In Table 5 the humidities and the maximum solubility in water for different saturated salt solutions have been listed. The values from these tables have been taken from QuantiFoils homepage [20]. The 20% RH environment was created by using Potassium acetate, Zinc nitrate gave 42% RH, Sodium bromide gave 60%, Sodium Chloride gave 76% RH and water gave 100 % RH. To control which relative humidity that was really obtained a humidity sensor was used. These sensors had a bias of +-2% RH. The controlled volume was made by plastic boxes with water-salt solutions at the bottom. In these boxes, metallic baskets contain the different specimen.

Table 5: The equilibrium humidities in an closed volume achieved by different salt and water solutions.

Salt	Expected relative humidity	Maximum solubility $[\frac{g}{100g\ water}]$
Potassium acetate	20%	247,6
Zinc nitrate	42%	558,4
Sodium nitrate	60%	90.6
Sodium Chloride	76%	36.0
Pure water	100%	-

Five samples for both Silica gel and activated alumina were prepared, weighed and marked. The specimens were then put in controlled environments which were sealed and left for at least 72 hours. The specimens could then be weighed to determine the amount of water adsorbed. The samples were taken from sealed containers with silica gel and activated alumina respectively, which gave homogeneous initial conditions for the materials. To get an absolute measurement of the water contents, the initial condition needs to be known. To do this, the density of dry activated alumina and silica gel had to be measured carefully. This was done by measuring a certain amount of material and drying this at 180 degrees Celsius in an oven. The weight of the material was measured both after and during the drying process. When no difference in weight could be detected during a one hour interval, the material was considered to be dry and the weight noted. The volume of the dried material was measured with help of a cone shaped container. The volume of the cone container was measured by filling it with water and measuring the weight. A cone shape was used to minimise the measuring errors. When measuring the volume of the material to be dried, it was vibrated into the container to fill it as much as possible. The cone volume was measured to 302ml+-0.5ml. From this a measurement of the density of vibrated dry silica and activated alumina could be determined.

The initial condition of the water content could then be determined by vibrating material into the cone with known volume and then weighed. The ratio between the measured density and the density of the dry material determines the initial water content. The result of the adsorption equilibrium curve mea-

surement is shown in Section 4.3

When measuring the relative humidities in the boxes, they were not approaching the predicted values and the humidity was very fluctuating. This made the results uncertain. Therefore Johan Forsgren at Uppsala University was contacted for better measurements of the adsorption of silica. It was later found that the humidity sensors used for the measurement were wrongly calibrated which resulted in high overestimation of the humidity in the middle range of the humidity spectrum. The measurement done by Forsgren was conducted by inserting a specimen of silica into a closed vessel where they could control the input of water molecules exactly. They could also measure the pressure in the vessel and thus the amount of water vapour. They let small portions of water into the chamber and then waiting for the specimen to adsorb it. If the specimen hadn't adsorbed the water in one minute the system was considered in equilibrium and a point on the adsorption curve was made. This continued until the whole relative humidity spectrum was covered. The result of this measurement is shown in 4.3.

These values were expected to be a bit lower than the true equilibrium values since a equilibrium already was expected after one minute. Thus the values from Forsgren's measurement were scaled so that the equilibrium water content for 100 % coincided with the a measurement of the equilibrium in 100% RH. This was done since the 100% RH measurement was considered to be the most accurate. A measurement of the water content increment depending on time was conducted to investigate the time evolution of the water content and to verify when equilibrium had occurred. The test was conducted for silica of two and four mm radius and also for two mm radius activated alumina.

For activated alumina, the equilibrium adsorption curve was found from a article investigating the temperature dependence of the adsorption curve of activated alumina F-200 [21]. This was compared to the measured values of the activated alumina. This can be seen in Section 4.3.

4 Results

4.1 Regeneration phase

In this section the simulated values are compared with the measured values for the three reference cases described in Section 3.2 and are shown in the Figures 5 to 16.

4.1.1 Case 1 - Constant temperature

In Figure 5 the requested effect,that is the PID-signal from the control unit to the heater device, is compared to the simulated input effect. It can be seen that the PID-signal is much more fluctuating but also that it continuously lies above the simulated value. This is also seen in Figure 6 where the simulated energy consumption thus lies below the requested effect from the regulation. The water transmission rate was fitted to release the right amount of water from the frame, that is the weight of the frame containing the hygroscopic material should be 610 grams lighter for the 100 degrees reference case and 800 grams lighter for the step change reference case. For the small box the change in frame weight has not been measured. Since the model is ideal in the sense that all water moisture higher than the saturation limit in the air is condensed and removed, the water production is thus expected to be overestimated when compared to the measured values. This is discussed in Section 5. In Figure 7 it can be seen that the total amount of condensed water is approximately 600 grams and that the measured values are substantially lower than this value. A scale and a delay are introduced to the simulated values to match the measured values. The scaled and delayed values of the water production is shown by the dotted line in Figure 7. This scale and delay were calculated to 74% and 500 seconds respectively. In Figure 8 the temperature in the centre of the frame is shown and it can be seen that the simulated temperature seems to rise faster than the measured temperature.

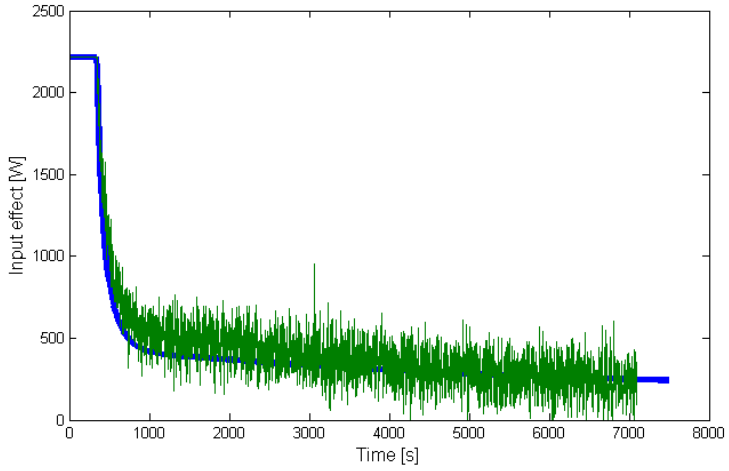

Figure 5: The input effect for Case 1, the 100 degrees regulation reference case. The PID-signal effect from regulation shown in green compared to the simulated input effect in blue.

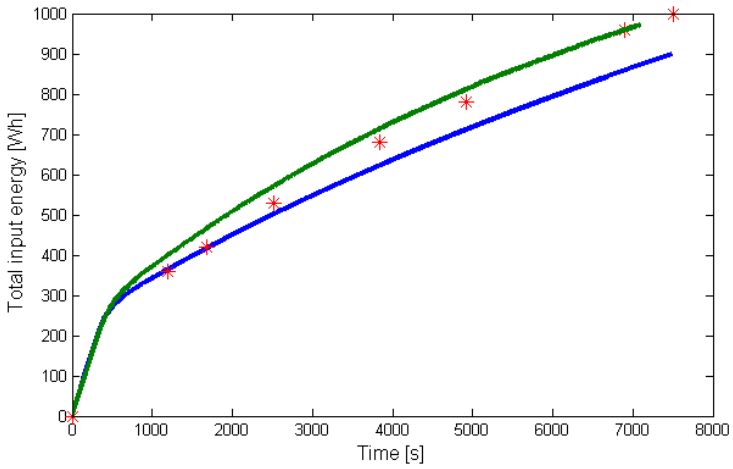

Figure 6: The energy consumption for Case 1, the 100 degrees regulation case. The integrated PID-signal effect from the regulation is shown in green. Measured values of the energy consumption is shown by red stars. The simulated energy consumption is shown in blue.

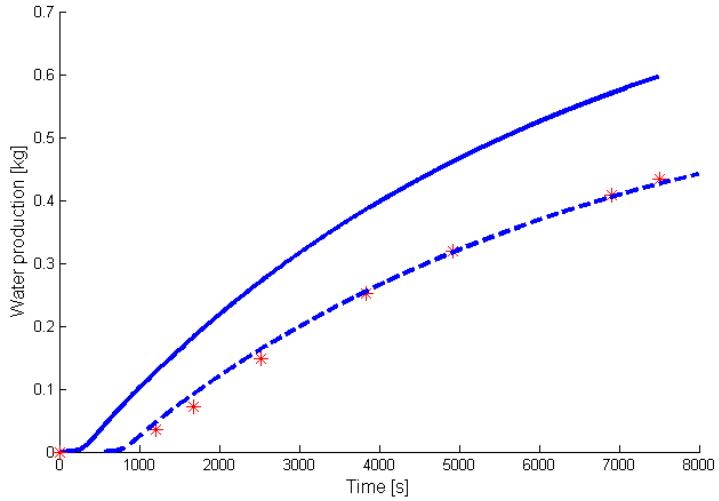

Figure 7: The water production for Case 1, the 100 degrees regulation case. The simulated values are shown in blue. The scaled and delayed simulated values are shown in dotted blue (See discussion in Section 5 about this). The measured values are shown in red.

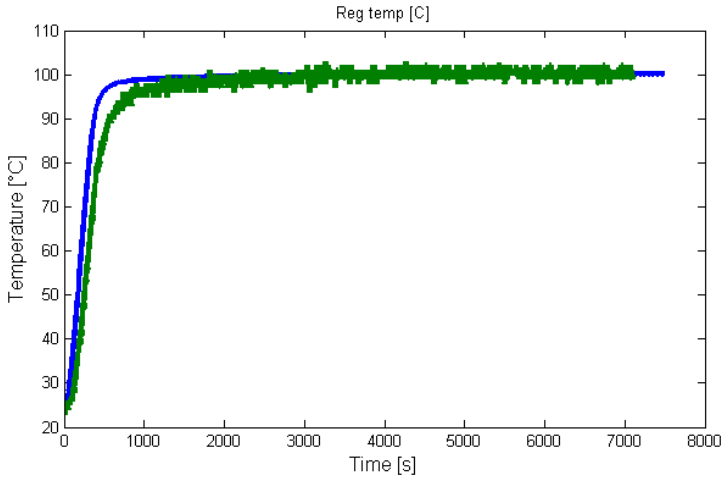

Figure 8: The regulation temperature in the centre of the frame for Case 1, the 100 degrees regulation case. The simulated values are shown in blue and the measured values are shown in green.

4.1.2 Case 2 - Temperature step change

Also in the the step change reference case the requested output effect is higher than the simulated values as seen in Figure 9. As in Case 1, the 100 degrees reference case, the values of the simulated energy consumption are lower than the measured values. In Figure 11 the total condensed water is approximately 790 grams which is much higher than the measured amount, but is coherent with the weight loss in the frame. The dotted line shows the scaled and delayed simulated values using the same scale and delay as for Case 1,the 100 degree reference case above, that is 74% and 500 seconds, respectively. This seems to give a good agreement with the measured values. The temperature rise is faster for the simulated system than for the measured system also for the step change reference case, as seen in Figure 12

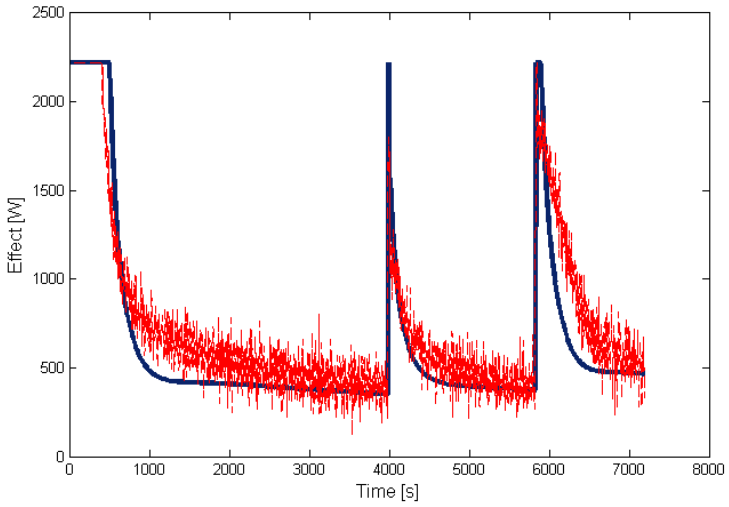

Figure 9: The input effect for Case 2, the step change regulation reference case. The PID-signal effect from regulation shown in red compared to the simulated input effect in blue.

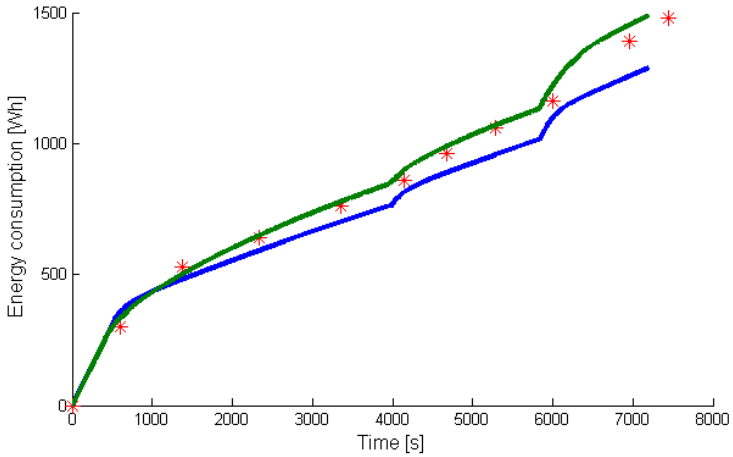

Figure 10: The energy consumption for Case 2, the step change regulation case. The integrated PID-signal effect from the regulation is shown in green. Measured values of the energy consumption is shown in red. The simulated energy consumption is shown in blue.

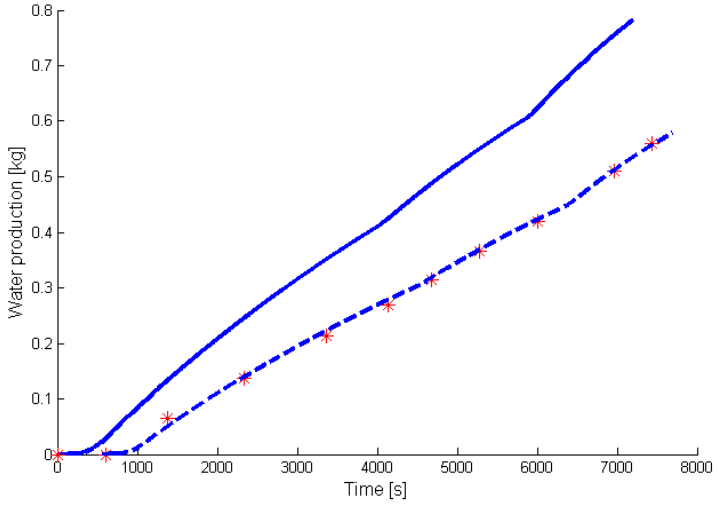

Figure 11: The water production for Case 2, the step change regulation case. The simulated values are shown in blue. Scaled simulated values are shown in dotted blue (See discussion in Section 5 about this). The measured values are shown in red.

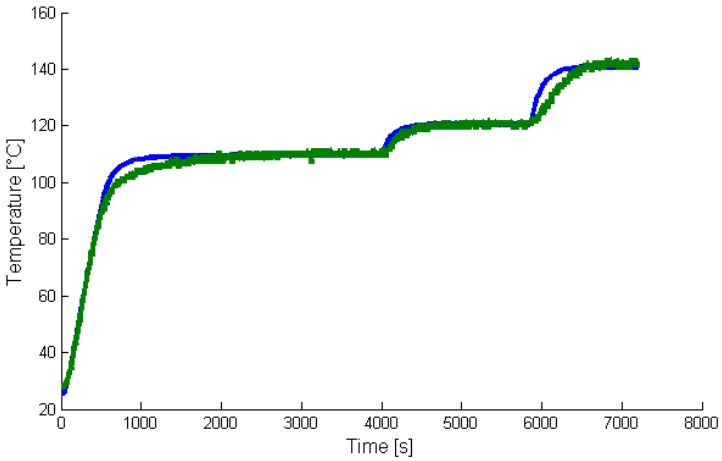

Figure 12: The regulation temperature in the centre of the frame for Case 2, the step change regulation case. The simulated value are shown in blue and the measured values are shown in green.

4.1.3 Case 3 - the smaller system

In the last test case the system was the smaller machine case, and the physical appearance of the system is significantly different from the other two cases. The PID-signal effect and the simulated input effect has a good agreement, but a smaller difference in the regulation oscillation, where the simulation is more oscillating, is noted in Figure 13. The energy consumption comparison in Figure 14 shows a very good agreement. The water production is expected to be greater in the simulation also in this case. The actual loss of water in the frame could unfortunately not be measured here. The scaled and delayed values for this system are found to be 83% and 130 seconds respectively, see Figure 15. The temperature rise and fall is slower for the simulated system as contrary to the other two test cases, which can be seen in Figure 16.

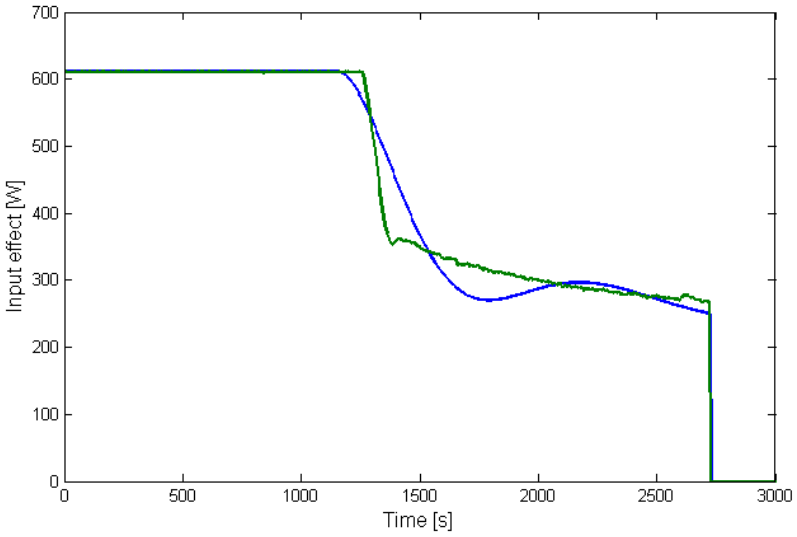

Figure 13: The input effect for Case 2, the small box reference case. The PID-signal effect from regulation shown in green compared to the simulated input effect in blue.

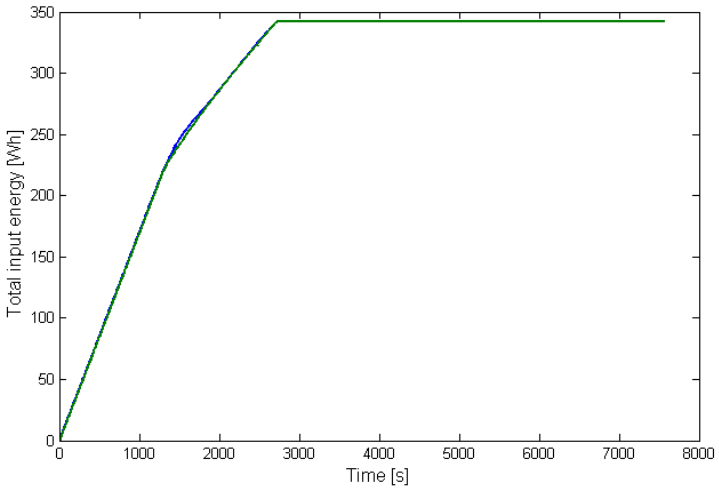

Figure 14: The energy consumption for Case 2, the small box reference case. The integrated PID-signal effect from the regulation is shown in green. The simulated energy consumption is shown in blue.

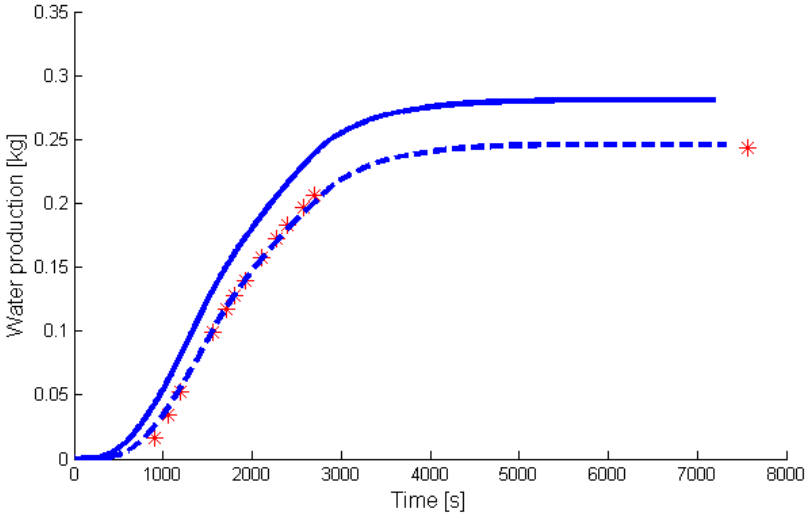

Figure 15: The water production for Case 2, the small box reference case. The simulated values are shown in blue. Scaled simulated values are shown in dotted blue (See discussion in Section 5 about this). The measured values are shown in red.

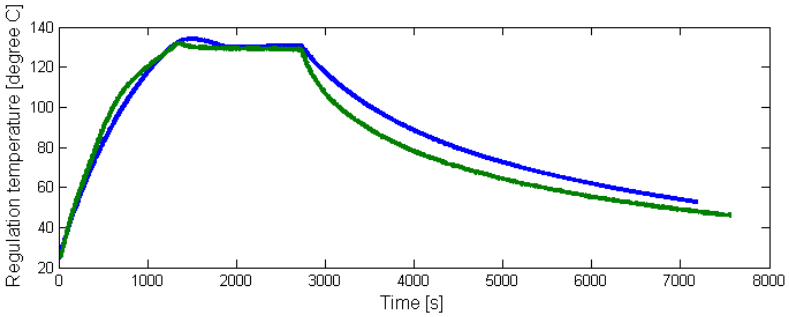

Figure 16: The regulation temperature in the centre of the frame for Case 3, the small box reference case. The simulated value are shown in blue and the measured values are shown in green.

4.2 Adsorption phase

In this section the simulation of the adsorption phase is compared to measured values of the temperature and the relative humidity during the adsorption phase. In Figure 17 the difference in moisture content between the inlet and the outlet is shown and is measured in mg water / kg air . There was clearly a bias in the measurement of temperature and relative humidity which leads to a bias

in the moisture content. After 14000 seconds the adsorption was considered negligible and this value was used to remove the bias. The red curve which is in good agreement with the simulation value is the measured values with the bias removed. In the sections where the measured values are zero there was no data in the output file for these times. Figure 18 compares the measured and the simulated values of the temperature in the centre of the frame. The simulated values are a bit delayed compared to the measured values but the peak has approximately the same amplitude. Figure 19 shows the outlet and inlet temperatures of the system. It can be seen that the simulated outlet temperature is a bit low compared to the measured. The measured values for the temperature are very square shaped because the values were measured and stored as integers. In Figure 20 the relative humidity of both the inlet and the outlet is shown and compared to the simulated values. We find that the inlet condition is not exactly constant at all time and that the simulated value is lower in the beginning. The bias can be seen here too since the difference in relative humidity should be zero after 14000 seconds, at least since there is no temperature difference.

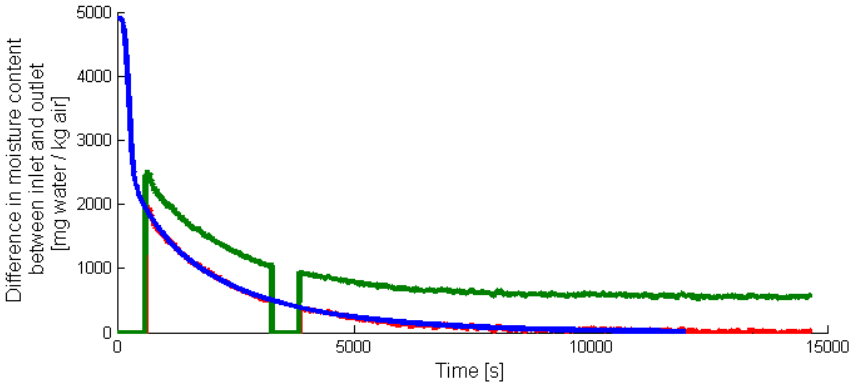

Figure 17: The difference in moisture content between the inlet and the outlet, measured in kg water per kg air. The blue line is the simulated values, the green line is the measured values and the red line is the measured values when removing the bias of 550 mg water / kg air.

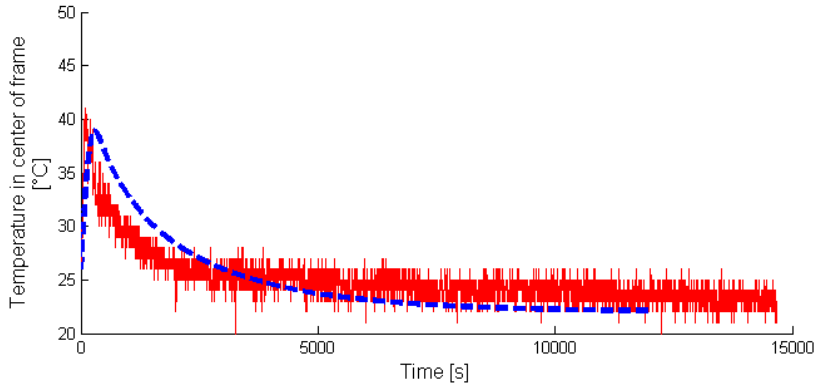

Figure 18: The temperature in the centre of the frame as a function of time. The simulated values in dotted blue are compared with the measured values in red.

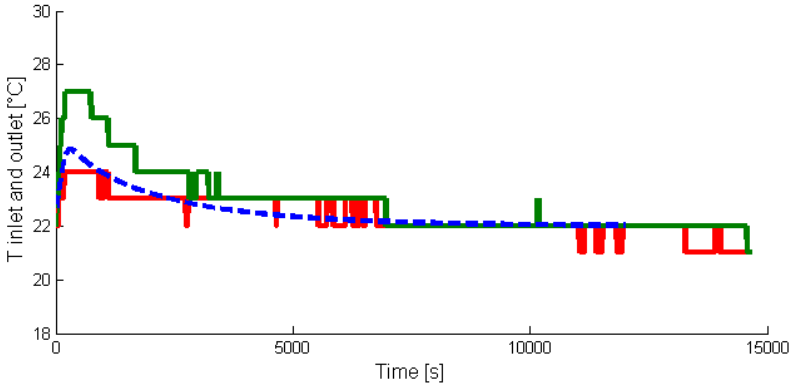

Figure 19: The temperature at both the inlet and the outlet. The simulated values for the outlet temperature are represented by the blue dotted line, which can be compared with the measured values for the outlet temperature shown in green. The measured inlet temperature is shown in red.

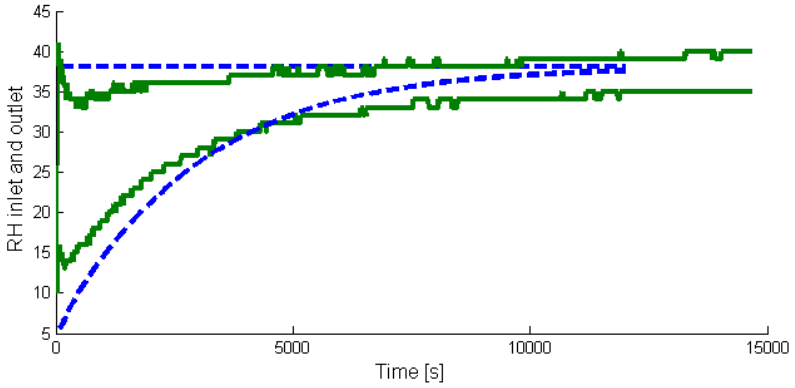

Figure 20: The simulated values of the relative humidity for both the inlet and the outlet compared with measured values. The blue dotted lines shows the simulated values and the green solid lines are measured values for both the inlet and the outlet.

4.3 Adsorption measurements

The results from the adsorption measurements are shown for silica gel and activated alumina, these are seen in Figure 21 and 22. The equilibrium water content in 100 % RH for a long time test is shown in Table 6

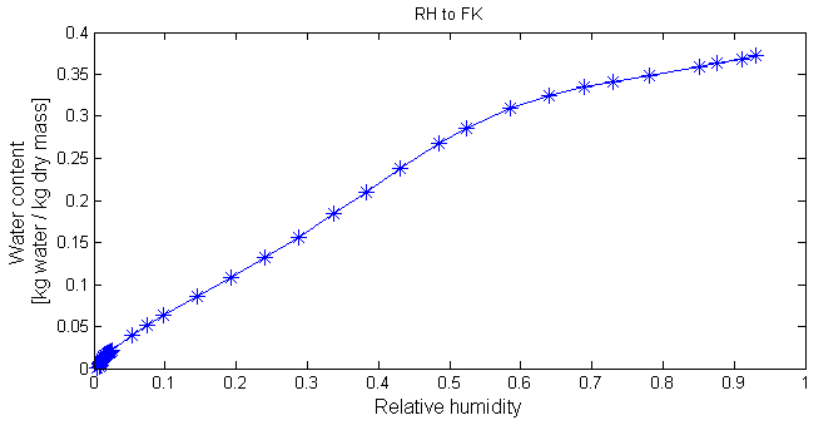

Figure 21: The adsorption curve measured by Johan Forsgren. The water content relative to the dry mass as a function of relative humidity.

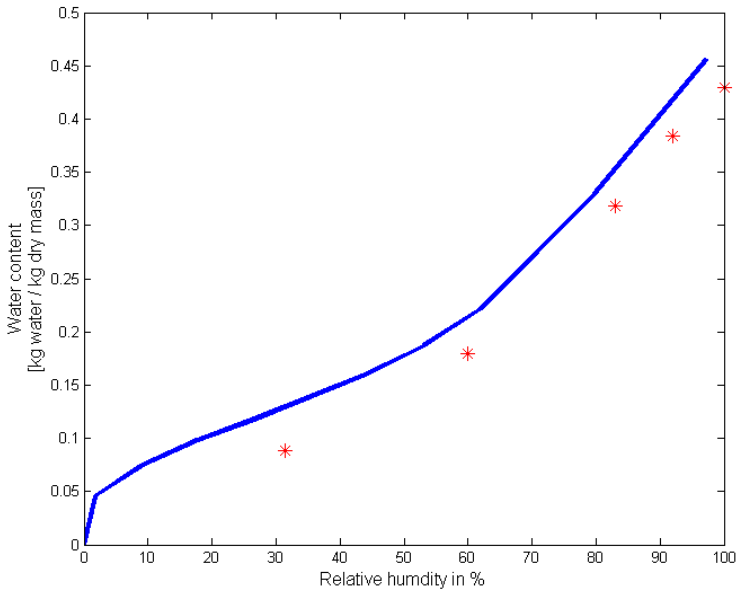

Figure 22: The adsorption curve taken from an article of activated alumina F-200 [21] shown in blue compared to the measured values of the used activated alumina shown by red stars. The water content relative to the dry mass as a function of relative humidity.

Table 6: The relative water content at equilibrum at 100 %

Hygroscopic material	Relative water content at equilibrium in 100 % relative humidity
SIlica 2mm	43.5
Silica 4mm	42.5
Activated alumina 2mm	42.5

5 Discussion

5.1 The regeneration phase

In Section 4.1 the results from the simulations are shown and compared with measured values. We find that for the two first cases, that is the 100 degree test case and the step change test case, the required input effect was lower than the actual one. Less energy was thus needed and the temperature rose more quickly. This could be due to different reasons but one reason is that the ideal model does not take into account all of the material in the machine that is heated. For example the top and the bottom of the machine is unaccounted for and the radiation pipes are not included. This would mostly be noticed during the temperature rise of the system and not during the maintenance phase where the input energy only needs to maintain the losses. It is also found in Figures 5 and 9 that the effect is lower also during the maintenance phase which could be due to an underestimation of outer or inner radiation, inner or outer convection or thermal conduction. It is also hard to estimate the active area of radiation and convection on the outside of the system. The system consists of more area used for convection and radiation than the model takes into account and the active part of this depends on the thermal conduction, i.e. how large area is heated to an extent that it gives non-negligible losses. To try to account for this, a scale factor could be estimated depending on the active area. To try to account for the increase in material a scale factor taking into account the weight of the real system could be used.

When trying to estimate the water production, the ideal model was used, that whenever the moisture content exceeded the saturation limit, the excessive amount of water was condensed and remove from the system. This is not true and thus there is a limit of how much water that can be condensed per second. If the pressure inside the vessel exceeds the atmospheric pressure, locally moisture will leave the system through gaps and the drainage pipe to level out the pressure difference. This will lead to a loss of water moisture. The fan that was used in the heating phase to protect the electronic devices was found to create a small flow inside the vessel and this were estimated to give rise to a moisture loss in the same order as the difference in water in the frame before and after the regeneration phase compared to the amount of condensed water. Since the system is not hermetically sealed, water moisture will also leave the system by diffusion.

The water transmission rate constant is fitted to release the right amount of water from the frame and as seen in Figures 7 and 11, the water production is vastly higher than the measured one. Most of the water leaving the frame condenses and leaves the system this way, which means that there is not a big difference between how much water that is removed from the frame and how much that is condensed on the walls. Since approximately 26% of the water should not be condensed, this means that there is a lot of energy that is given back to the system, via the evaporation energy of water, which not is the case in reality. This could account for a part of the underestimation made on the

energy input before.

In this model the natural convection that is taking place inside the vessel can be described by the Nusselt number to avoid the modulation of a three dimensional flow. The correctness of this is uncertain and the effect that this has on mass and energy transport could be underestimated. Also it can be seen in Figures 7 and 11 that it seems as if there is a delay between the model and the measurements. This could be because the model removes the condensed water directly from the system and in reality small drops needs to form and then be transported on the wall and to a hole before it leaves the system. So by fitting the results by using a delay and a scale factor on the water production the delay of 500 seconds and scale factor of 74% were achieved. Theses values are interesting since they give a good agreement to both the 100 degree test case and the step change test case. These two test cases are made with the same system and the scale and delay factor could be a system property. In the case of the small system, the energy production was in good agreement and the water was less overestimated, about 14%, compared to the 35% for the other two cases. This could be an indication that the smaller system does not have as large losses as the bigger system.

To get a better simulation, more sophisticated models for transport of heat and mass both in air and inside the hygroscopic materials would be needed, but the main improvement would probably be to implement a better model of the condensation process and to try to predict the leakage. The rate at which the water condenses on a surface is discussed by Eames et al [22] and Pound et al[23] and could be a subject for future improvement of the model. Other driving forces have also been used to model the rate of water evaporation from the hygroscopic material. The difference between the actual water content and the equilibrium water content has been used by Zhang et al [24] and Sakoda et al [25] and [26]. Yao et al [27] uses the difference in humidity as a driving force for the water transmission. To use the difference in vapour pressure seems to be the most promising, but the other methods could be to preferred as a simplification in certain cases.

5.2 The adsorption phase

The measurements during the adsorption phase clearly have a bias, and there are both systematic and accuracy errors during measurements when using all of the sensors. The specified accuracy from the manufacturer was $\pm$ 2% for the relative humidity sensors and much less for the temperature sensors. For the temperature the important thing is the systematic error where the probe could be put at different locations during different measurements leading to unreliable results. It can be seen in Figure 20 that there still is a difference in relative humidity on the in and outlet after the 14000 seconds. Part of the difference can be explained by temperature difference, but unfortunately the logging device was wrongly programmed and thus only saving integers for both relative humidity and temperature, which made it hard to correct for this. Even a small change in temperature due to for example heat losses in

the fan can have a big influence on the saturation steam pressure and thus on the relative humidity, but that could not be detected now. The difference in moisture content in the air is also expected to go to zero, see Figure 17. This did not happen and the uptake stagnated at a value of 550mg water / kg air. After 14000 seconds we expect the value to be zero and therefore the 550mg was considered a bias in the measurements. It is still not easy to verify if it is the outlet or the inlet that is wrongly calibrated or both. When removing the bias the simulation has a very good agreement with the measured results. The temperature in the material also gives a very similar behaviour and increases to 40 degrees Celsius when the uptake is at the maximum as seen in Figure 18. The simulated outlet temperature is lower than expected from measurements. The model uses estimations of heat and mass transfer numbers during the interaction with the hygroscopic material. These values and also the values of the specific area of the hygroscopic material are sensitive. If for example the heat transfer between the gaseous phase and the solid phase were to be increased, then the temperature of the gas would increase and thus lower the temperature of the material bed. Also if the mass transfer number would be increased, the amount of water that is adsorbed is higher and thus the amount of energy deposited from the condensation. To fit the data better the heat and mass transfer numbers were altered. The results from the simulation indicates that it includes the proper physics but more measurements are needed to verify the model.

5.3 Adsorption measurements

The measurement of the adsorption curve is a bit uncertain since the simple method using equilibrium salt solutions did not work as well as expected. The measurements from Uppsala University were lower than those values that were measured with the equilibrium salt solutions. This led to the scaling of 15% of the adsorption curve of silica so that the value for 100% relative humidity was matched. This would be correct if the equilibrium achieved after one minute is at a relative distance from the true equilibrium, that is the same for all humidities. The measurements for the activated aluminium were consistently lower than the values achieved from the article. This could be due to the fact that the activated alumina used in this experiment is not as dry as the species in the article. This is also a fact that is true for the adsorption curve of silica. If the silica would not be considered completely dry then, this would effect the measurements of the adsorption curve.

5.4 General discussion

When creating this model the objective was to try to understand the process of the CMCR method and see how well the process could be reproduced using basic models describing the different phases. This gives more insight in which parts that are important for the process and how this can be used.

Overall the model could produce a similar result as measured and catch the basic phenomena, giving an estimation of the energy input within 10% and a

water production within 35% of the measured values for all test cases. The PID regulation of the simulation coefficients were also the same as in the measurements, and since the regulation is similar the system could also be considered similar. The water production is overestimated which also is expected since a reliable model for the condensation has not been implemented. For the bigger system the water production gave a much better agreement for both of the test cases when scaling with 74% and a delay of 500 seconds.

The model could be used to give an estimation of the result when changing parameters in the system, i.e. testing new hygroscopic materials, new materials to be used in the frame or other ways of regulation. Environmental changes could also be investigated using this model i.e. changing the ambient temperature or humidity. The adsorption phase model can be used to estimate how much the material can adsorb in different environments in a certain time frame. How long time the adsorption phase and regeneration phase should be respectively, could also be investigated with this model.

6 Conclusions

A model for the CMCR process is proposed. The regeneration phase and the adsorption phase have been modelled separately using basic equations describing heat transfer and mass transfer. Peng et al [7] and Sun et al [14] were reference articles for the model. The water transmission between the air and the hygroscopic material were modelled with the difference in vapour pressure as a linear driving force.

The characteristic curves for adsorption were measured with simple methods and with help of Uppsala University for the specific types of silica gel and activated alumina that were used during the project. The simple way of measuring the adsorption curve was uncertain, partly due to wrongly calibrated sensors used. The calibrated measurements from Uppsala were instead used.

The energy input was underestimated during the regeneration phase and the water production was over estimated. The over estimation of the water production was probably due to an improper model for the condensation process and the lack of a model for the leakage. The results could therefore potentially be improved in the model. The water production also had a delay which could be explained by the transport time of water in the real system. Using a delay and a scale of 500 seconds and 74% made the water production agree well with the measurements of the main apparatus. The smaller system seemed to have less losses if the model were to be trusted. The adsorption rate inside the material was modelled with good agreement and the temperature rise in the material resembled the measured data but was a bit delayed compared to this. The temperature rise in the gas was a bit low compared to the measured one and the difference in relative humidity was overestimated in the beginning of the adsorption. The results from the simulation of the adsorption indicate that it includes the proper physics but more measurements are needed to validate the model.

References

[1] Pernilla Johansson, Thomas Svensson, and Annika Ekstrand-Tobin. Validation of critical moisture conditions for mould growth on building materials. *Building and Environment*, 62(0):201 – 209, 2013. doi: 10.1016/j.buildenv.2013.01.012.

[2] Jong Won Choi, Gilbong Lee, and Min Soo Kim. Numerical study on the steady state and transient performance of a multi-type heat pump system. *International Journal of Refrigeration*, 34(2):429 – 443, 2011. doi: http://dx.doi.org/10.1016/j.ijrefrig.2010.09.021.

[3] V.R. Tarnawski and P.K. Yuet. Winter performance of residential heat pump. *Heat Recovery Systems and {CHP}*, 8(3):271 – 278, 1988. doi: http://dx.doi.org/10.1016/0890-4332(88)90063-4.

[4] C.R. Ruivo, A. Carrillo-Andrés, J.J. Costa, and F. Domínguez-Muñoz. A new approach to the effectiveness method for the simulation of desiccant wheels with variable inlet states and airflows rates. *Applied Thermal Engineering*, 58(1–2):670 – 678, 2013. doi: http://dx.doi.org/10.1016/j.applthermaleng.2011.12.052.

[5] Stefano De Antonellis, Cesare Maria Joppolo, and Luca Molinaroli. Simulation, performance analysis and optimization of desiccant wheels. *Energy and Buildings*, 42(9):1386 – 1393, 2010. doi: http://dx.doi.org/10.1016/j.enbuild.2010.03.007.

[6] Napoleon Enteria, Hiroshi Yoshino, Akira Satake, Akashi Mochida, Rie Takaki, Ryuichiro Yoshie, Tiruaki Mitamura, and Seizo Baba. Experimental heat and mass transfer of the separated and coupled rotating desiccant wheel and heat wheel. *Experimental Thermal and Fluid Science*, 34(5):603 – 615, 2010. doi: http://dx.doi.org/10.1016/j.expthermflusci.2009.12.001.

[7] Shi-Wen Pen, Robert W. Besant, and Graeme Strathdee. Heat and mass transfer in granular potash fertilizer with a surface dissolution reaction. *The Canadian Journal of Chemical Engineering*, 78(6):1076–1086, 2000. ISSN 1939-019X. doi: 10.1002/cjce.5450780607.

[8] Lucia Ferrari, Josef Kaufmann, Frank Winnefeld, and Johann Plank. Interaction of cement model systems with superplasticizers investigated by atomic force microscopy, zeta potential, and adsorption measurements. *J Colloid Interface Sci*, 347(1):15–24, 2010.

[9] Ryoji Takahashi, Satoshi Sato, Toshiaki Sodesawa, Machiko Kawakita, and Katsuyuki Ogura. High surface-area silica with controlled pore size prepared from nanocomposite of silica and citric acid. *The Journal of Physical Chemistry B*, 104(51):12184–12191, 2000. doi: 10.1021/jp002662g.

[10] Ahmad A. Pesaran and Anthony F. Mills. Moisture transport in silica gel packed beds—i.theoretical study. *International Journal of Heat and Mass Transfer*, 30(6):1037 – 1049, 1987. doi: http://dx.doi.org/10.1016/0017-9310(87)90034-2.

[11] Yunus A. Cengel. *Heat Transfer: A Practical Approach*. Mcgraw-Hill (Tx), 2nd edition, November 2002.

[12] Amir Faghri, Yuwen Zhang, and John Howell. *Advanced Heat and Mass Transfer*. Global Digital Press, 2010.

[13] Nellis Gregory and Sanford Klein. Cambridge University Press, 2008. doi: http://dx.doi.org/10.1017/CBO9780511841606.012.

[14] Jin Sun and Robert W. Besant. Heat and mass transfer during silica gel–moisture interactions. *International Journal of Heat and Mass Transfer*, 48(23–24):4953 – 4962, 2005. doi: 10.1016/j.ijheatmasstransfer.2005.02.043.

[15] Robert. Schirmer. Die Diffusionszahl von Wasserdampf-Luft-Gemischen und die Verdampfungsgeschwindigkeit. *Verfahrenstechnik*, (6):170 – 177, 1938.

[16] W. Wagner and A. Pruss. International equations for the saturation properties of ordinary water substance revised according to the international temperature scale of 1990 (vol 16, pg 893, 1987). *Journal of physical and chemical reference data*, 22(3):783–787, 1993.

[17] M.A. Rady, A.S. Huzayyin, E. Arquis, P. Monneyron, C. Lebot, and E. Palomo. Study of heat and mass transfer in a dehumidifying desiccant bed with macro-encapsulated phase change materials. *Renewable Energy*, 34(3):718 – 726, 2009. doi: http://dx.doi.org/10.1016/j.renene.2008.04.038.

[18] M. Punčochář and J. Drahoš. The tortuosity concept in fixed and fluidized bed. *Chemical Engineering Science*, 48(11):2173 – 2175, 1993. doi: http://dx.doi.org/10.1016/0009-2509(93)80092-5.

[19] Jonathan E. Guyer, Daniel Wheeler, and James A. Warren. FiPy: Partial differential equations with Python. *Computing in Science & Engineering*, 11(3):6–15, 2009. doi: 10.1109/MCSE.2009.52.

[20] QUANTIFOIL Instruments. Creating constant air humidity in closed vessels, July 2013.

[21] Atanas Serbezov. Adsorption equilibrium of water vapor on f-200 activated alumina. *Journal of Chemical & Engineering Data*, 48(2):421–425, 2003. doi: 10.1021/je025616d.

[22] I.W. Eames, N.J. Marr, and H. Sabir. The evaporation coefficient of water: a review. *International Journal of Heat and Mass Transfer*, 40(12):2963 – 2973, 1997. doi: http://dx.doi.org/10.1016/S0017-9310(96)00339-0.

[23] G. M. Pound. Selected values of evaporation and condensation coefficients for simple substances. *Journal of Physical and Chemical Reference Data*, 1(1):135–146, 1972. doi: 10.1063/1.3253096.

[24] Li Zhi Zhang and Ling Wang. Effects of coupled heat and mass transfers in adsorbent on the performance of a waste heat adsorption cooling unit. *Applied Thermal Engineering*, 19(2):195 – 215, 1999. doi: http://dx.doi.org/10.1016/S1359-4311(98)00023-4.

[25] A. Sakoda and M. Suzuki. Simultaneous transport of heat and adsorbate in closed type adsorption cooling. *Journal of Solar Energy Engineering*, 108(3):239–245, 1986. doi: 10.1115/1.3268099.

[26] A. Sakoda and M. Suzuki. Fundamental study on solar powered adsorption cooling system cooling. *Journal of chemical engineering of Japan*, 17(1): 52–57, 1984.

[27] Ye Yao, Weijiang Zhang, Kun Yang, Shiqing Liu, and Beixing He. Theoretical model on the heat and mass transfer in silica gel packed beds during the regeneration assisted by high-intensity ultrasound. *International Journal of Heat and Mass Transfer*, 55(23–24):7133 – 7143, 2012. doi: http://dx.doi.org/10.1016/j.ijheatmasstransfer.2012.07.028.